Available *online* at : http://jnte.ft.unand.ac.id/

Jurnal Nasional Teknik Elektro

| ISSN (Print) 2302-2949 | ISSN (Online) 2407-7267 |

Fault Detection and Diagnosis of a 3-Phase Induction Motor Using Kohonen Self-Organising Map

Robert Agyare Ofosu [1], B. Odoi[2], D. F. Boateng[2], A. M. Muhia[3,4]

[1]*School of Electrical and Information Engineering, Jiangsu University, Zhenjiang, China*
[2]*Department of Mathematical Sciences, University of Mines and Technology, Tarkwa, Ghana*
[3]*Department of Electrical and Electronic Engineering, University of Mines and Technology, Tarkwa, Ghana*
[4]*Department of Electrical and Electronic Engineering, Jomo Kenyatta University of Agriculture and Technology, Nairobi, Kenya*

ARTICLE INFORMATION

Received: Augustus 19, 2022
Revised: December 12, 2022
Available online: March 31, 2023

KEYWORDS

Induction Motor, Kohonen Self-Organising Map, Fault Detection and Diagnosis, Accuracy

CORRESPONDENCE

Phone: +233540358161
E-mail: raofosu@umat.edu.gh

A B S T R A C T

This paper uses the Kohonen Self-Organising Map (KSOM) to detect, diagnose, and classify induction motor faults. A series of simulations using models of the 3-phase induction motor based on real industrial motor parameters were performed using MATLAB/Simulink under fault conditions such as inter-turn, power frequency variation, over-voltage and unbalance in supply voltage. The model was trained using the input signals of the various fault conditions. Various faults from an unseen induction motor were fed to the model to test the model's ability to detect and classify induction motor faults. The KSOM adapted to the conditions of the unseen motor, detected, diagnosed and classified these faults with an accuracy of 94.12%.

INTRODUCTION

An Induction Motor (IM) is an Alternating Current (AC) electromechanical machine that converts energy from electrical to mechanical. Induction motors are reliable, rugged and almost unbreakable with an estimated efficiency above 80% [1]. Though, induction motors are very reliable, nevertheless, due to harsh environmental conditions and installations, they are susceptible to several types of faults [2]. Hence, the maintenance of induction motors has become the main challenge that many industries face now to prevent unscheduled downtime and reduce maintenance costs [3], [4].

According to Gheitasi [5], the petrochemical industry in the United States of America (USA) alone, accumulated approximately $ 20 billion in annual losses, due to poor diagnostic approach to detecting and diagnosing faults in induction motors. Therefore, a proper approach to fault detection and diagnosis of induction motors has become increasingly essential. Over the years, most of these faults including stator, rotor and bearing faults have been dealt with using several diagnostic approaches. Artificial intelligence-based techniques, Hilbert Transform (HT), Discrete Wavelet Transform (DWT) and chemical analysis are some of the recently proposed techniques for the detection and diagnosis of induction motor faults [6]. However, these techniques were not very successful because, at low loads, analysing the faults using these techniques was difficult due to the closeness of the defect's frequency to the fundamental frequency. Furthermore, Hilbert Transforms technique though has proven to be effective in detecting faults in induction motors, they are difficult to implement due to the complex mathematical computations while other techniques like the chemical approach could handle only a few fault conditions such as the bearing faults [7], [8], [9].

Moreover, techniques such as the Motor Current Signature Analysis (MCSA) require sensors to be fitted in the induction motors to acquire useful signals [10]. These sensors interfere with the normal operation of induction motors and make the technique expensive due to the additional cost. Fuzzy logic control algorithm has also been used successfully in the fault detection of induction motors [11], [12]. Although the algorithm was able to indicate the condition of the induction motor with high accuracy, the limitation however, had to do with the system's inability to adapt to new fault conditions.

Upon the review of related literature on the various techniques of detecting and diagnosing faults in the induction motor, it was

https://doi.org/10.25077/jnte.v12n1.1047.2023

realised that no work has been done using a single intelligent approach to detect, diagnose and classify several induction motor faults simultaneously with a faster computational time and higher accuracy. Because of these challenges, an online intelligent-based system is proposed using Kohonen Self-Organising Map (KSOM) to address these problems. KSOM does not require sensors for its implementation, can self-learn and self-improve to adapt to new conditions of the induction motor. Moreover, the size of the map can be increased to handle any number of faults conditions and also possesses visualisation capabilities. As such, the KSOM can be used as a successful diagnostic technique for the detection and diagnosis of induction motor faults.

Classification of Induction Motor Faults

Faults in 3-phase induction motors can be categorised into electrical, mechanical and environmental faults [3]. Electrical faults can be divided into single phasing, over and under voltage, unbalance in supply voltage, inter-turn short circuit and power frequency variation faults. Broken rotor bar, bearing damage, rotor mass unbalance and air gap eccentricity are some classifications of mechanical faults. Ambient temperature, external moisture, vibration of motor due to installation defects and foundation defects affecting the performance of the induction motor are classified under environmental faults. The percentage failure components of the induction motor are shown in Figure 1 [5]. These were surveys conducted by the Institutes of Electrical and Electronics Engineers (IEEE) and the Electric Power Research Institute (EPRI). From Figure 1, it can be observed that the major induction motor faults occur inside the stator windings as well as the rotating shaft.

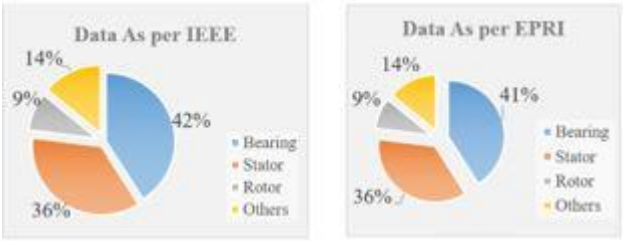

Figure. 1. Percentage of Various Induction Motor Faults

Electrical Faults

These faults are classified as stator and rotor faults. They occur mainly in the windings especially in the stator windings since they are more susceptible to faults. Figure 2 shows a diagram of a damaged stator winding of a 3-phase induction motor [8].

Figure 2. Damaged Stator of a 3-Phase Induction Motor

As a result of the stator coil and rotor striking the stator of the induction motor, the top sticks may loosen and damage the copper conductors and their insulation, thereby resulting in stator winding faults. Also, if due to power fluctuations the induction motor is subjected to a number of starts and stops, the temperature of the windings will rise above the temperature limit of the induction motor and consequently destroy the motor insulation. Figure 3 is a diagram of burnt stator windings due to inter-turn short-circuit and short-circuit between the stator winding and stator core [13].

(a) Short-Circuit Between Winding and Core

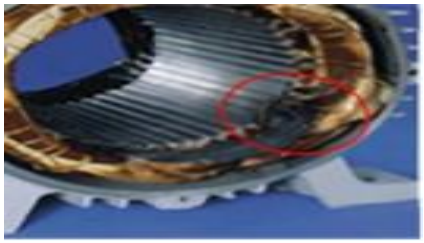

(b) Inter-Turn Fault

Figure 3. Burnt Stator Windings Due to Stator Faults

Mechanical Faults

According to the survey conducted by the Electric Power Research Institute (EPRI), it was deduced that mechanical faults contributed to approximately 41% of induction motor faults. Broken rotor bar and rotor mass unbalance are the main mechanical faults. Broken rotor bar faults in 3-phase induction motors occur when a bar of the rotor of an induction motor is broken partially or completely. This is mainly caused by the addition of heavy end rings to the rotor construction which introduce large centrifugal forces with extra stresses that may cause the breakage of the rotor bar [9]. Moreover, if the motor is made to run for a longer period, any of the bars of the rotor may get cracked. This introduces the asymmetrical distribution of rotor currents. As such, there will be overheating in the cracked part which may eventually cause the breakage of the bar. Consequently, the other sidebars will be made to carry a higher amount of current as a result of the breakage of the single bar and this may subject the sidebars to larger mechanical and thermal stresses [7]. If the motor is allowed to run in this condition for a longer period, the sidebars may also get cracked and thus, damage may spread through the entire rotor causing the breakage of multiple bars. The main effect of broken rotor bar is the introduction of a ripple effect in the torque and speed of the motor [7]. This ripple effect can be computed using (1) [8].

$$f_r = f(1 \pm 2ks) \quad (1)$$

Rotor mass unbalance is caused by a phenomenon called air-gap eccentricity. This occurs when the rotor is not aligned centrally to the stator, thereby causing a non-identical air-gap between the rotor and stator of the induction motor. Air-gap eccentricity causes the side of the rotor where there is a minimum air gap to experience greater electromagnetic pull while the opposite with maximum air-gap experiences lower electromagnetic pull and

hence, occurrence of rotor mass unbalance [9]. This electromagnetic pull that comes into play as a result of air-gap eccentricity may cause the rotor and stator to rub against each other. Consequently, due to friction, part of the rotor may wear out and cause rotor mass unbalance fault as shown in Figure 4.

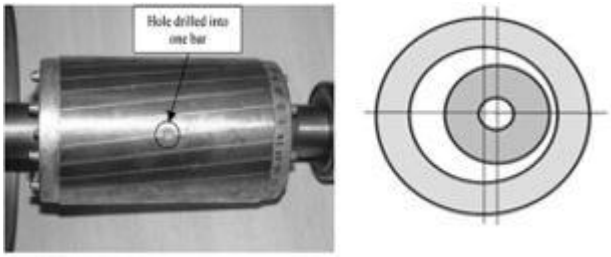

(a) Pitting on Rotor Bar (b) Rotor Eccentricity

Figure 4. Rotor with Mass Unbalance Fault

The main effect of rotor mass unbalance is that there will be oscillation in the air-gap. This variation in the air-gap will cause variations as it is been induced in the stator winding. Consequently, the induced voltage variation will also cause stator current harmonics which can be computed in (2) [7].

$$f_s = f\left[\frac{k(1-s)}{p}\right]+1 \tag{2}$$

Kohonen Self-Organising Map

KSOM is a special class of Artificial Neural Network (ANN) that transforms complex high dimensional input data into simpler and easy to visualise output without loss of information. KSOM can deal with missing data, small-sized data and data with unlimited size. KSOM learns without being supervised; thus, it does not rely on predefined target outcomes to guide its learning but rather learns by observation. In order to be unsupervised, the neurons of the KSOM compete against themselves for the opportunity to present the characteristics of the input data. The formation of the KSOM algorithm involves steps as summarised in the flow chart of Figure 5.

From the KSOM algorithm, the distance between the input and the output data is computed using (3) [14] as:

$$d_i = \|x(t) - w_i(t)\| \tag{3}$$

After computing the distance, the winning output neuron is computed using the minimum Euclidean criterion given in (4) [14]

$$c(t) = \arg\min \left\{\|x(t) - w_i\|\right\} \tag{4}$$

KSOM has only two layers: Input and output layers connected by their associated weight vectors. The input layer neurons represent the variables of the input data.

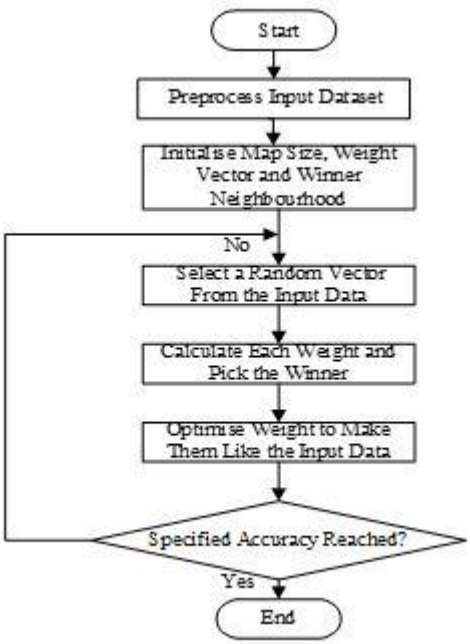

Figure 5. Flowchart of Kohonen-Self Organising Map

Figure 6 is a graphical representation of the KSOM. In training the KSOM, a batch training algorithm is preferred [14]. In batch training, the whole dataset is used to train the map simultaneously. The batch training algorithm has no time-variable learning rate parameter, therefore, making the batch training algorithm faster than any other training algorithm [14]. In using the batch training algorithm, 2-phase learning namely, coarse training and fine training are utilised in training the KSOM. The input dataset is first trained using coarse training after which the fine training phase continues until the corrections to the KSOM become approximately zero.

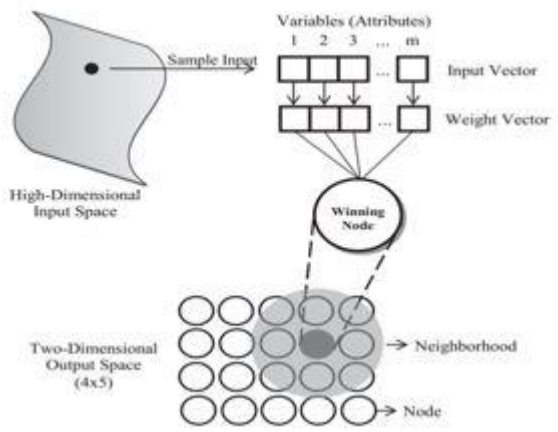

Figure 6. Graphical Representation of KSOM

Accuracy of the KSOM is the ability of the SOM to produce simpler, easy to visualise low dimensional representations of complex high dimensional data without information loss during the process. Quantisation Error (QE) is utilised in determining how accurate each condition of the induction motor would fit onto the KSOM. The accuracy and error of the SOM in terms of its ability to represent each condition of the induction motor on the map are computed using (5) and (6) [14] as:

$$QE = 1/T \tag{5}$$

$$Acurracy = (1 - QE) \times 100 \tag{6}$$

https://doi.org/10.25077/jnte.v12n1.1047.2023

METHOD

In this paper, the KSOM was utilised as a diagnostic tool for detecting, diagnosing and classifying faults in the 3-phase induction motor. Firstly, using MATLAB/Simulink software, the induction motor was modelled in both healthy and faulty conditions. The stator current which is a characteristic of an induction motor condition was the priority. The KSOM should be able to efficiently learn and extract all the characteristics of each condition of the modelled induction motor. To replicate the exact condition on a 2-dimensional map once that condition is detected and diagnosed, the 3-phase rotor currents, speed and torque together with the 3-phase stator currents were acquired from the modelled induction motor and were stored as a MATLAB dataset. The acquired dataset from the induction motor was then fed to the KSOM for training and validation. The KSOM then extracted all the features from the induction motor dataset and classified each condition on a 2-dimensional map for the purpose of visualisation.

Model Design of 3-Phase Induction Motor

The usefulness of the modelling equations was realised in the MATLAB/Simulink model of the 3-phase induction motor [4]. Preset models of the induction motor have been provided in MATLAB/Simulink and these models have parameters based on the modelling equations that mimic the real industrial induction motor. In this paper, the parameters of the preset model of the 3-phase induction motor that was utilised in the simulations is provided in Table 1.

Table 1. Model Parameters of 3-Phase Induction Motor

Parameter	Value
Power (kW)	4
RMS Voltage (V)	400
Frequency (Hz)	50
Rotor Speed (RPM)	1430
Stator Resistance (Ω)	1.405
Rotor Resistance (Ω)	1.395
Stator Inductance (H)	0.005839
Rotor Inductance (H)	0.005839
Mutual Inductance (H)	0.1722
Pole Pairs	2
Input Mechanical Load Torque (Nm)	26.72
Peak Voltage (V)	326.54
Rotor Inertia (kgm^2)	0.0131

For the selected preset model as specified in Table 1 to mimic a real induction motor, a 3-phase voltage source block was used as the supply to the induction motor. The source was connected in a star configuration with each of the three phases having a peak value of 326.6 V, a frequency of 50 Hz and displaced 120° from each other. The peak value of each phase was as a result of the induction motor having a 400 V RMS rating and was computed using (7) [15].

$$V_p = \frac{V_{rms}\sqrt{2}}{\sqrt{3}} \quad (7)$$

The supply passed through a 3-phase VI measurement block before it was fed to the induction motor. The VI block measured the 3-phase voltage and current of the voltage source. Scope and display blocks were connected to the VI block to show the voltage and current values.

When the induction motor was ran, the 3-phase stator currents, rotor currents, speed and torque generated were displayed in the three scopes labelled stator currents, rotor currents, speed and torque, respectively. The gain block connected to the speed and torque scopes converted the speed of the induction motor from radians per second to revolutions per minute. The speed in radians per second was multiplied in the gain block to get the speed in revolutions per minute. The stator currents, rotor currents, speed and torque were stored as a MATLAB file and fed to the designed KSOM model. The Simulink model of the designed system is shown in Figure 7.

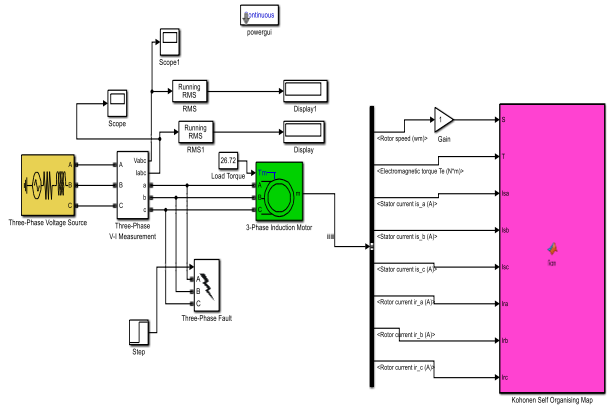

Figure 7. Simulink Model of the Designed System

Design of the Kohonen Self-Organising Map

The design of the KSOM model was done by using programming codes from the SOM toolbox imported into MATLAB/Simulink. The toolbox had inbuilt functions that were used to implement the KSOM algorithm. Flow chart of the KSOM of how the codes were written in creating, training and validating the KSOM model is shown in Figure 8.

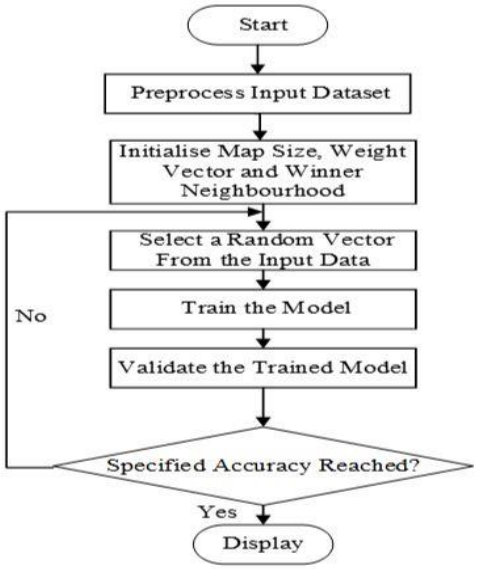

Figure 8. Flow chart of the Developed Kohonen Self-Organising Map

Pre-Processing of Induction Motor Input Dataset

The input dataset namely, the 3-phase stator currents, 3-phase rotor currents, speed and torque of the induction motor that represented each of the modelled operational conditions of the induction motor were pre-processed by dividing each of the input samples by the highest value in the sample. Each of the input datasets had its own unit of measurement as such, the pre-processing was done to bring all the input datasets to a common scale and also to ensure that the input dataset was verified and validated and did not contain any outliers that may have been caused by systematic errors.

Initialising the Kohonen Self-Organising Map

In the initialisation stage, the size of the map, the shape of the neurons, the neighbourhood radius as well as the number of epochs which represented the number of times the model was trained were all defined. The map size was set to a two-dimensional unit neuron map. This size was chosen to make the map large enough in order to accommodate all the input dataset that represented the various operating conditions of the induction motor. The neurons were arranged on the map to represent a low-dimensional projection of the features of each of the operational conditions of the induction motor. The shape of the neurons was chosen to be hexagonal. The hexagonal shape was chosen because, it was the shape that was able to accommodate all the features of a sample from the input dataset that represented an operational condition of the induction motor.

The neighbourhood radius that defines the neighbours of each of the neurons was set to 0.4. This value was chosen because it was the accepted value that was utilised in the toolbox for SOM implementation. The number of epochs that represented the number of times the KSOM was trained was set to 50 and 10 for the first and second phases of training, respectively. Figure 9 is a diagram of the initialised KSOM.

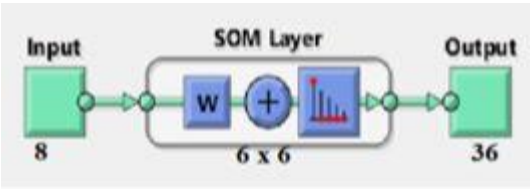

Figure 9. Initialised Kohonen Self-Organising Map

Training the Kohonen Self-Organising Map

The KSOM was trained for the map to learn each of the operational conditions of the induction motor from the input dataset. Batch computation was employed for the training of the map. The numerical values of stator currents, rotor currents, speed as well as torque obtained during the simulation of the designed model under various operational conditions of the induction motor were utilised in training the KSOM. A total of 8 input samples as shown in Figure. 9 with each representing an operational condition of the induction motor were used for the training. For a faster computational time, the batch training algorithm was divided into two training phases namely, coarse training and fine training.

During the coarse training, the weight vectors that served as links between the input dataset and the output of the neurons of the map were randomly selected from the input data set. Because the learning process did not depend on predefined target outcomes that guided the learning process, the output neurons of the map had to compete against themselves in order to represent the input dataset on the output of the map. To find the output neurons that best represented the features which were the stator currents, rotor currents, speed and torque of the input dataset, the distance between the input dataset and the weight vectors were computed using the Euclidean distance method given in (3).

After computing the distance, the winning output neuron was computed using the minimum Euclidean criterion given in (4). The weight vectors associated with the winning neurons and its neighbouring neurons were adjusted to become more representative of the features that characterised the input dataset. This was done by using the batch training algorithm given in (8) [14] as:

$$m_i(t+1) = \frac{\sum_{j=i}^{n} h_i(t) x_j}{\sum_{j=1}^{n} h_i(t)} \tag{8}$$

Validating the Kohonen Self-Organising Map

To ascertain whether or not the trained KSOM would be able to detect, diagnose to know the type of condition of the induction motor, whether healthy or faulty and classify the various conditions of the induction motor on the same 2-dimensional map, an induction motor different from the one used to train the KSOM was modelled under various fault conditions and the dataset in terms of stator currents, rotor currents, speed and torque were acquired and labelled as the dataset from an unseen induction motor. The training dataset and the dataset from the unseen motor were combined to form a total of 17 input samples and were then fed to the trained KSOM for fault detection and classification.

Accuracy of the Kohonen Self-Organising Map

The accuracy of the KSOM had to do with the ability of the map to produce simpler, easy to visualise low dimensional representations of complex high dimensional input datasets that were utilised for the map's training and validation without information loss during the process. The accuracies of both the training and the validating datasets were calculated mathematically using quantisation error as shown in (5) and (6).

Simulation of Induction Motor Faults

After the normal operation of the 3-phase induction motor had been simulated, the simulation of the various faults that the 3-phase induction motor can be susceptible to, was next in line. The faults that were simulated were; power frequency variation, single phasing, over voltage, voltage unbalance, single phase to ground short-circuit, 2-phase to ground short-circuit, 3-phase to ground short-circuit and inter-turn short circuit. In each fault condition, the stator current, rotor current, speed and torque of the induction

https://doi.org/10.25077/jnte.v12n1.1047.2023

motor were recorded and stored as a dataset. Rotor faults were not simulated but rather it was the stator side of the induction motor that was simulated and fed to the KSOM due to the fact that any fault occurring in the rotor would produce a corresponding signature in the stator by transformer action. In all the faults simulated, the stator current, rotor current, speed and torque of the induction motor were recorded between 0.2 and 2 seconds after steady state of the induction motor were achieved.

Power Frequency Variation Fault

In practice, the frequency of the supply of the 3-phase induction motor is supposed to be 50 Hz, any frequency other than this will subject the 3-phase induction motor to power frequency variation fault. This fault was simulated by changing the frequency of the preset model of the induction motor from 50 Hz to 60 Hz.

Single Phasing Fault

Single phasing fault occurs in practice, when any of the three phases of the stator winding is lost, in effect making that particular phase's voltage equivalent to zero [16]. The single phasing fault was simulated by setting any one of the phases of the preset induction motor to zero.

Unbalance in Supply Voltage

Different magnitudes of voltage in any one of the three phases of supply lead to voltage unbalance fault, as each of the phases of the supply must have equal magnitudes. In practice, a blown fuse in any of the phases of the supply causes a voltage unbalance fault. Fault due to unbalance in supply voltage was simulated by only changing the voltage magnitude in any one of the phases of the voltage supply to the preset 3-phase induction motor model. A change in voltage magnitude above or below in any of the phases of the supply may lead to failure of the 3-phase induction motor, as such unbalance in supply voltage fault was created by reducing phase A of the supply voltage by 6%, increasing the phase B of the supply by 8% and reducing the phase C of the supply by 10% and the results were computed in (9) [15] as:

$$V_{Ra} = V_a - \left(V_a \times \frac{6}{100} \right) \tag{9}$$

$$V_{Ra} = 326.60 - \left(326.60 \times \frac{6}{100} \right)$$

$$V_{Ra} = 307.004 \text{ V}$$

Over Voltage

In practice, a phase voltage in the stator windings greater than the rated voltage results in over voltage fault. When any of the phases of the supply voltage has a voltage greater than the rated voltage of the 3-phase induction motor this fault emerges. A change in voltage magnitude in any of the phases of the 3-phase induction motor above 5% leads to failure of the induction motor. As such, the over voltage fault was simulated by increasing the magnitude of phase A of the supply voltage by 6% and the results were computed in (10) [15] as:

$$V_{Ra} = V_a + \left(V_a \times \frac{6}{100} \right) \tag{10}$$

$$V_{Ra} = 326.60 + \left(326.60 \times \frac{6}{100} \right)$$

$$V_{Ra} = 346.196 \text{ V}$$

Single Phase to Ground Short-Circuit Fault

In practice, a single phase to ground fault occurs when there is a leakage current path between any of the phases of the stator winding input voltage and the ground. Single phase to ground fault was simulated by short-circuiting any of the input phases to ground using the 3-phase fault block in Figure 7.

2-Phase to Ground Short-Circuit Fault

When any two of the stator phases are shorted causing current to be channelled to ground, 2-phase to ground short-circuit fault occurs in practice. This fault was simulated by selecting any two phases and the ground from the 3-phase fault block connected to the induction motor model in Figure7. This caused the current to be channelled from the two selected input phases to the ground causing current to be supplied from the unselected input phase only to the induction motor.

3-Phase to Ground Short-Circuit Fault

When all the phases of the input were shorted causing all or greater percentage of the stator current to be channelled to the ground, then this fault occurred. Simulation of 3-phase to ground short-circuit fault was done by short-circuiting all the phases of the input voltage to ground by way of selecting all the phases and the ground in the 3-phase fault block in Figure7.

Inter-Turn Short-Circuit Fault

Inter-turn short-circuit occurs between turns of the same slots of the stator winding. The resistance and inductance of the stator of the preset 3-phase induction motor in Figure 7 were 1.405 Ω and 0.005839 H, respectively. These values of resistance and inductance were what was obtained when the motor is operating under normal conditions. To simulate the 3-phase induction motor under inter-turn short-circuit fault, (11) [15] was utilised as:

$$\frac{R_{stator,normal}}{R_{stator,\,fault}} = \eta = \frac{L_{stator,normal}}{L_{stator,\,fault}} \tag{11}$$

The value of $R_{stator,\,fault}$ was assumed to be 0.008 Ω which is extremely less than $R_{stator,normal}$. The small value of $R_{stator,\,fault}$ implies that, the stator resistance has reduced extremely and thus, more stator current can flow through the stator windings. Thus, the value of stator fault inductance was computed using (11) ([15] as:

$$L_{stator,\,fault} = \frac{0.005839 \times 0.008}{1.405} = 0.00003325\ H \tag{12}$$

The 3-phase induction motor was operated normally however, after 0.2 seconds, the faulted stator resistance and inductance were replaced with the normal stator resistance and inductance, respectively. After 1 second, the stator current, rotor current, speed and torque of the induction motor were read and recorded.

Unseen 3-Phase Induction Motor

To ascertain whether or not the trained KSOM would be able to detect, diagnose and classify faults in any other 3-phase induction motor apart from the induction motor that was utilised for its training, another 3-phase induction motor based on parameters of a real industrial motor was modelled. Afterward, power frequency variation, single phasing, over voltage, voltage unbalance, single phase to ground short-circuit, 2-phase to ground short-circuit, 3-phase to ground short-circuit and inter-turn short circuit faults were simulated. The 3-phase stator currents, rotor currents, speed and torque of each fault condition were recorded to form a total of 9 induction motor input datasets. The 9-input samples with each representing a fault condition were then fed to the trained KSOM for fault detection and classification. The model parameters that were used in modelling the unseen motor has been provided in Table 2.

Table 2. Model Parameters of 3-phase Induction Motor

Parameter	Value
Power (kW)	15
RMS Voltage (V)	400
Frequency (Hz)	50
Rotor Speed (RPM)	1460
Stator Resistance (Ω)	0.5968
Rotor Resistance (Ω)	0.6258
Stator Inductance (H)	0.0003495
Rotor Inductance (H)	0.005473
Mutual Inductance (H)	0.354
Pole Pairs	2
Input Mechanical Load Torque (Nm)	98.12
Peak Voltage (V)	326.54

RESULTS AND DISCUSSION

The 3-phase induction motor was successfully modelled in healthy and faulty conditions using MATLAB/Simulink. The results in terms of stator currents, rotor currents, speed and torque of the motor were presented in the form of graphs and the findings of the research were discussed.

Results for Normal Operation of the 3-Phase Induction Motor

The 3-phase stator currents, rotor currents, speed and torque are indicative of the health of the 3-phase induction motor. Figure 10, Figure. 11 and Figure. 12 are the graphs of the 3-phase stator currents, rotor currents, speed and torque of the healthy 3-phase IM, respectively.

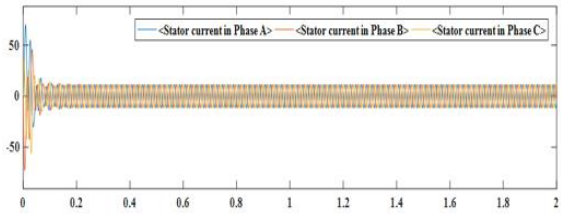

Figure 10. 3-Phase Stator Currents of Healthy Induction Motor

After 0.1 seconds, steady-state was reached and the stator currents were perfectly sinusoidal. The stator currents also had the same amplitude in all the 3-phases. This is indicative of the healthy state of the motor.

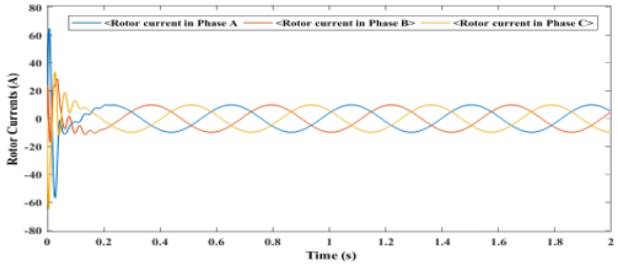

Figure 11. 3-Phase Rotor Currents of Healthy Induction Motor

The rotor currents had fewer cycles due to slip. However, after steady state was attained, all the phases had the same amplitude and perfectly sinusoidal, which is indicative of the healthy state of the induction motor.

The 3-phase induction motor model utilised, had a rated speed of 1430 RPM. After the steady-state was reached, the expectation was that the speed of the heathy 3-phase induction motor reaches its rated speed of 1430 RPM and stays in that state without any fluctuation. The torque of the induction motor was also expected to reach a constant value of 26.7 Nm and stay in that state throughout the whole time without any fluctuations. All these features that are indicative of the healthy condition of the induction motor were exhibited in the speed and torque of the 3-phase induction motor graph in Figure. 12.

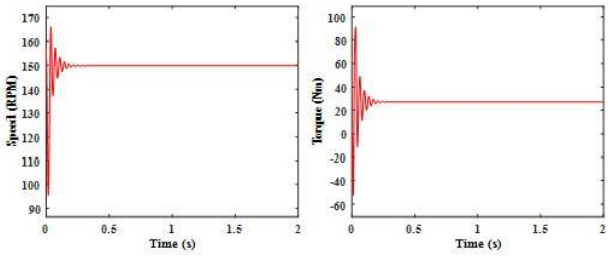

Figure. 12 Speed and Torque of the Healthy 3-Phase Induction Motor

Results Of Various Induction Motor Faults Simulations

The results obtained from simulating the 3-phase induction motor under various fault conditions are presented as follows:

Power Frequency Variation Fault

https://doi.org/10.25077/jnte.v12n1.1047.2023

When this fault was simulated, the magnitudes of the stator and rotor currents as well as the magnitudes of the speed and torque of the motor compared to that of the healthy motor were increased. This was as a result of the increased magnitude of the output voltage and voltage drop of the motor. Eventually, this may lead to core losses and poor efficiency which may cause the load-carrying capacity of the induction motor to reduce. Comparing the graphs of the stator and rotor currents in Figure 13 under power frequency variation to that of the motor in healthy condition, it can be seen that the number of cycles is increased in this case thereby, causing a lot of fluctuations in the system. Figure. 13 is the graph of the stator and rotor currents, respectively under the power frequency variation fault.

The corresponding graphs of speed and torque graphs of the induction motor under power frequency variation are given in Figure 14. The recorded values of speed and torque were 1460 RPM and 26.62 Nm, respectively. It can be seen that these values deviated from that of the healthy induction motor and this was as a result of the increased frequency. The increased frequency caused the speed to increase dangerously while the torque decreased.

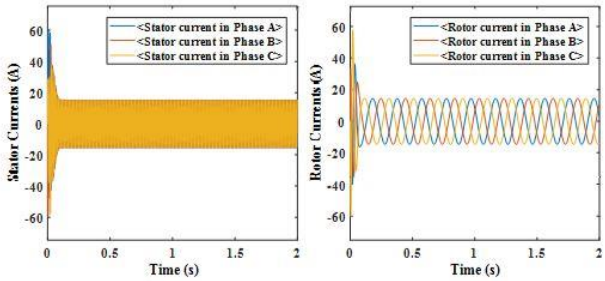

Figure. 13 3-Phase stator and rotor currents under power frequency variation fault

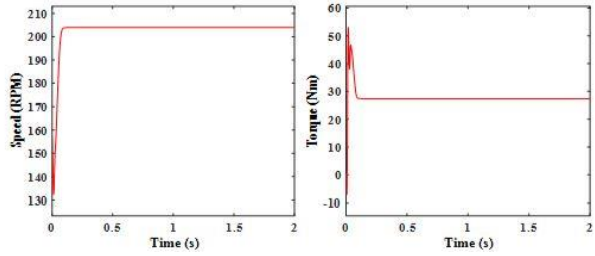

Figure 14. Speed and Torque of Induction Motor under Power Frequency Variation

Single Phasing Faults

When single phasing fault was simulated, the magnitude of the stator and rotor currents of the opened phase becomes small. The currents in the other two phases, however, increased to approximately 2.4 times greater than the nominal currents of the healthy induction motor. Single phasing fault can subject the induction motor to vibrations and noise due to uneven torque produced in the air-gab of motor. Comparing the graphs of the stator and rotor currents of the motor under single phasing to that of the motor under healthy conditions, it can be seen that the stator and rotor currents in single phasing are not perfectly sinusoidal but rather pulsating. Figure 15 is the graphs of the stator and rotor currents under single phasing fault.

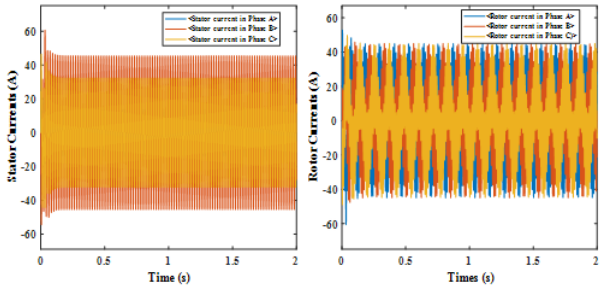

Figure 15. 3-Phase Stator and Rotor Currents under Single Phasing Fault

The corresponding speed and torque graphs obtained under this condition are given in Figure 16. From the graph, the values of speed and torque were 1424 RPM and 28.82 Nm which are deviations from that of the healthy induction motor. Due to differences in flux between the stator and rotor, the speed and torque pulsated and their waveforms were not sinusoidal.

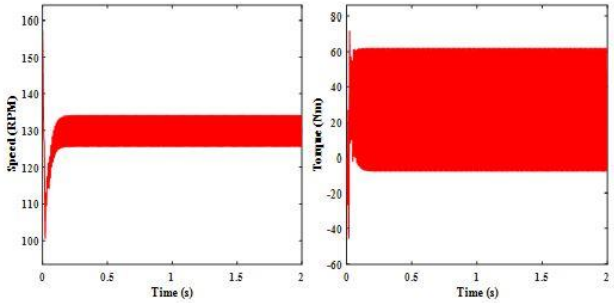

Figure. 16. Speed and torque of motor under single phasing fault

Unbalanced Voltage Supply Fault

The fault of unbalanced supply voltage caused the stator and rotor currents to be unbalanced. The unbalanced currents resolved into positive, negative and zero sequence components. The positive sequence currents produced positive torque and the negative sequence currents produced negative torque opposite the direction of the positive sequence torque. The net torque got reduced due to the effect of unbalanced stator currents. Comparing the graphs of the stator and rotor currents in Figure. 17 to that of the motor under healthy condition, it can be seen that under unbalanced voltage the currents in each phase have different magnitudes and also are pulsating. This fault causes overheating which can eventually result into burning of the motor windings. Figure 17 is the graph of the stator and rotor currents, respectively under unbalanced voltage supply fault conditions.

The corresponding speed and torque graphs obtained under this condition are shown in Figure. 18. The speed of the motor under unbalance voltage fault pulsated and reduced from the normal to 1420 RPM. The torque also oscillated dangerously due the unbalanced voltage that was supplied to the motor.

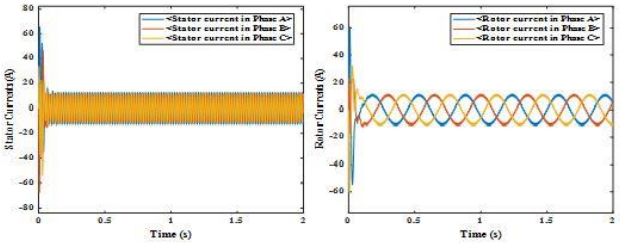

Figure 17 3-Phase Stator and Rotor Currents of Motor Under Unbalanced Supply Voltage

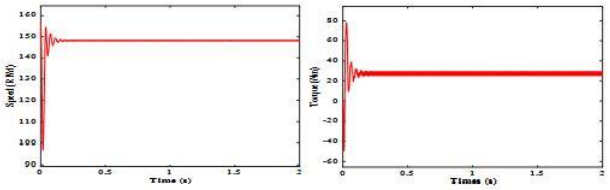

Fig. 18 Speed and Torque of Induction Motor under Unbalance Voltage

Over Voltage Fault

When the over voltage fault occurred, the stator and rotor currents magnitude became higher due to the fact that the motor was ran at a voltage higher than its rated voltage. This may lead to the generation of noise and vibration in motor. The motor may end up with more losses due to the drawing of high currents and reduced efficiency. Comparing the graphs of the stator and rotor currents under this condition to that of the motor under healthy condition, it can be seen that the magnitudes of currents under this condition are higher, pulsating and not perfectly sinusoidal. Figure 19 is a graph of the stator and rotor currents, respectively of the motor under over voltage fault condition.

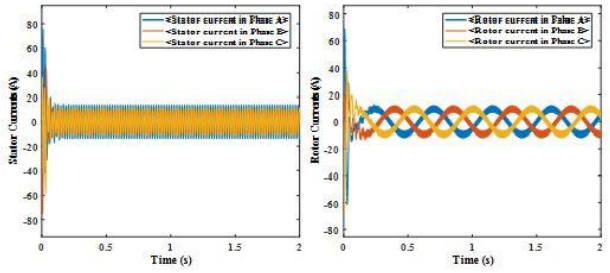

Figure. 19 3-Phase stator and rotor currents of induction motor under over voltage

Single Phase to Ground Short-Circuit Fault

A short-circuit is a direct contact between two points of different electrical potentials. When this fault was simulated 0.5 seconds after the normal running of the motor, there was a sudden surge of current in the phase that was shorted to ground. As such, the stator and rotor current magnitudes in each phase were different, pulsating and not perfectly sinusoidal which was as a result of the difference between the stator and rotor fluxes. This condition may lead to the generation of excessive heat which may eventually damage the motor. Figure 20 is a graph of the stator and rotor currents, respectively of the motor under single phase short-circuit fault.

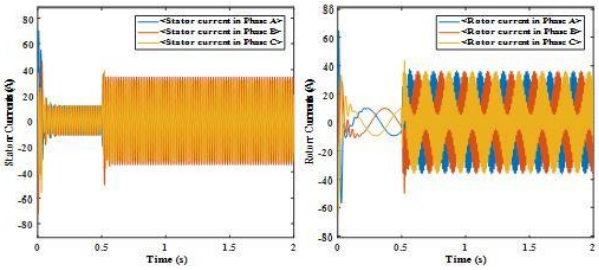

Figure 20. 3-Phase Stator and Rotor Currents of Motor Under Phase short-circuit

2-Phase to Ground Short-Circuit Fault

Any two phases of the motor were shorted to ground. Consequently, an excessive amount of current was drawn from the supply voltage. The stator and rotor currents exhibited irregularities in their waveform patterns as compared to that of the motor under healthy condition during the entire time when the fault was inserted. Figure 21 is the graphs of the stator and rotor currents, respectively of the motor under 2-phase to ground short-circuit. fault.

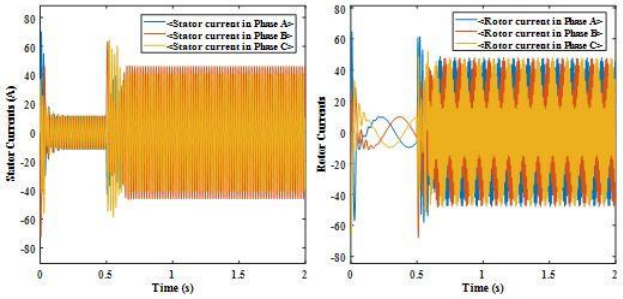

Figure. 21 3-Phase Stator and Rotor Currents of Motor Under 2-Phase Short-Circuit

3-Phase to Ground Short-Circuit Fault

After running the induction motor for half a second, all the three phases of the supply voltage were shorted to ground. As such, the stator and rotor of the motor received a small amount of current. The stator and rotor of the motor would not have received any current at all if the fault were allowed to persist thereby bringing the motor to a standstill eventually. The graphs of the stator and rotor currents of the motor under this condition is shown in Figure 22.

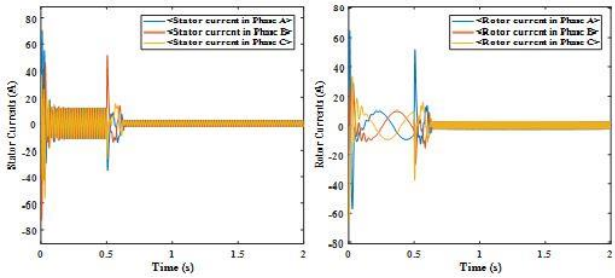

Figure 22. 3-Phase Stator and Rotor Currents of Motor Under 3-Phase Short-Circuit

https://doi.org/10.25077/jnte.v12n1.1047.2023

Inter-Turn Short-Circuit Fault

From the stator and rotor currents graphs shown in Figure. 23, it can be seen that when this fault occurred, the magnitudes of the stator and rotor currents went dangerously high as opposed to when the motor was running under healthy conditions. This fault when allowed to persist for a significant amount of time may cause overheating of motor windings, generate sparks, vibration, high noise levels and eventual damage of motor.

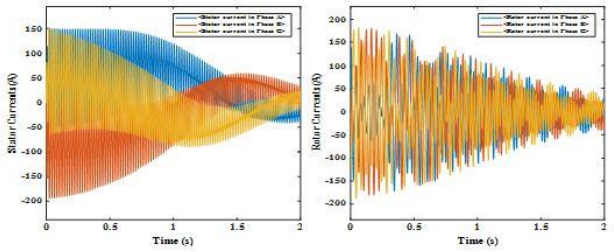

Figure. 23 3-Phase Stator and Rotor Currents Under Motor Inter-Turn Fault

Results of Training and Validation of the Model

The numerical values of stator currents, rotor currents, speed as well as torque obtained during the simulation of the designed model under various operational conditions of the induction motor were utilised in training the KSOM. A total of 9 input samples with each sample representing a different operational condition of the 3-phase induction motor were utilised in training the model. The model used 20 seconds to learn each of the conditions of the inputs that were utilised for its training.

Using quantisation error, the error in terms of the trained model's ability to represent each operational condition of the 3-phase induction motor was calculated to be 11.11% and thus, the overall accuracy of the trained model was calculated to be 88.89%. This error was as a result of only 9 inputs used to train the model. This implied that a larger number of inputs representing the operational conditions of the induction motor fed to the model would increase the model's accuracy, as the error is inversely proportional to the number of inputs. To validate the trained model, a preset induction motor labelled as an "unseen motor" different from the induction motor that was used to train the SOM, was modelled using MATLAB/Simulink in different operational conditions. A total of 8 input samples with each sample representing an operational condition on the induction motor was utilised in validating the trained model.

The training dataset together with the dataset from the unseen induction motor, collectively resulted into 17 input samples, with each sample representing an operational condition of the 3-phase induction motor were fed to the trained model to ascertain how the trained KSOM would adapt to the unseen motor and detect, diagnose and classify each fault condition on a 2-dimensional map, for easy identification and visualisation. The results of the model's detection and classification of faults on a 2-dimensional map are shown in Figure 24.

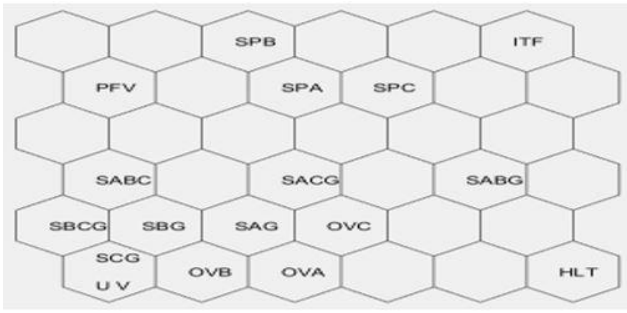

Figure. 24 Results of the Model's Detection and Classification of Faults

Discussion of Results

The KSOM algorithm proved that faults in 3-phase induction motors could be easily detected, diagnosed to know the kind of fault and the results displayed on a 2-dimensional map for identification and visualisation. In training the SOM with the 8 input samples, the batch computation was utilised in the algorithm, as such it was observed that it took approximately 20 seconds for the KSOM to learn and extracted all the features of the various operating conditions of the 3-phase induction motor. After the 8 input samples were used to train the SOM, the overall accuracy for the trained KSOM was calculated to be 88.89%. After feeding the trained SOM with both the training and datasets from the unseen induction motor, the model was able to adapt to the new conditions of the unseen motor, detected and classified the various faults using only 0.5 seconds while the accuracy of the output of the model was also calculated to be 94.12% which is an improvement on accuracy of that of the training dataset. The accuracy increased from 88.89% to 94.12% because the number of input samples also increased from 8 to 17 sample respectively. This proves that as the number of inputs increased, the error reduced and thus, the accuracy of the model increased.

From the map shown in Figure. 24, it was observed that the healthy condition of the induction motor was classified on the bottom right corner of the map as "HLT" with no other condition closer to it, and as such it was differentiated from the other conditions. Because the numerical values of stator and rotor currents, speed and torque of the induction motor in inter-turn short circuit fault condition were dangerously high, it was classified at the top right corner of the map as "ITF" and thus was totally differentiated from the other conditions. Power frequency variation was also clearly classified on the map as "PFV" with no other condition closer to it.

Single phase short-circuit to ground in phases A, B and C (SAG, SBG, SCG), 2 phase short-circuit in phases A, B and C (SABG, SACG, SBCG), 3-phase short-circuit in all 3 phases (SABC), over voltages in Phases A, B, C (OVA, OVB, OVC) as well as unbalance in supply voltage (UV) faults were all classified at the bottom left corner of the map with each of these conditions being the neighbour of the other, thereby an indication of their similarities. However, short-circuit fault in phase C (SCG) and unbalance in supply voltage (UV) faults were both classified on the same node at the bottommost left corner of the map, indicating that, they both had the same statistical features.

CONCLUSIONS

Kohonen Self-Organising Map Model has been successfully designed to detect, diagnose and classify induction faults. it has been shown that the trained KSOM adapted to the conditions of an unseen induction motor, detected and classified the faults in the unseen motor with a computational time of 0.5 seconds and an accuracy of 94.12% and the size of the map can be increased to accommodate any number of induction motor conditions, either healthy or faulty. It is therefore recommended that this technique should be employed in the control rooms of industries to monitor the health of induction motors to detect and diagnose faults even while they develop.

ACKNOWLEDGMENT

The authors appreciate Jiangsu University, University of Mines and Technology and Jomo Kenyatta University of Agriculture and Technology for making available the necessary resources for the completion of this research work.

REFERENCES

[1] C. Y. Eduardo, A. F. Arturo, G. Arturo, J. R. Rene and M. L. Jose, "Real-time condition monitoring of vsd-fed induction motors through statistical analysis and synchronous speed observation", *International Transactions on Electrical Energy Systems*, Vol. 5, No. 8, pp. 1-15, 2015.

[2] A. Soualhi, G. Clerc and A. Lebaroud, "Fault detection and diagnosis of induction motors based on hidden markov model", *IEEE Transactions*, Vol. 20, No. 2, pp. 1-7, 2012.

[3] W. J. Bradley, "Current-based fault detection and diagnosis of induction motors", Ph.D. dissertation, University of Bradford, England, 2013.

[4] V. H. Nguyen, "Model-based diagnosis and prognosis of induction motors under stator winding fault", Ph.D. dissertation, Nanyang Technological University, Singapore, 2018.

[5] A. Gheitasi, "Motor fault recognition using distributed current signature analysis", Ph.D. dissertation, Auckland University of Technology, New Zealand, 2013.

[6] L. Dezhi, "An intelligent system for induction motor health condition monitoring", Ph.D. dissertation, University of Waterloo, Canada, 2015.

[7] H., A. Talhaoui, A. K. Menacer, and T. Ameid, "Experimental diagnosis of broken rotor bar fault in induction motor based on hilbert and discrete wavelet transforms", *International Journal of Advanced Manufacturing Technology*, Vol. 22, No. 12, pp. 1-11, 2017.

[8] S. C. Karmakar, M. Surajit, M. Mitra and S. Senguta, "Induction motor fault diagnosis: approach through current signature analysis", *IEEE Journal of Industry Applications*, Vol. 2, No. 7, pp. 30 – 32, 2016.

[9] M. Rahman, and M. N. Uddin, "Online unbalanced rotor fault detection of an induction motor drive based on both time and frequency domain analyses", *IEEE Transactions on Industry Applications*, Vol. 15, No. 5, pp. 1-11, 2016.

[10] S. Sarkar and Hembram, P. K. "Acquisition and pre-processing of three phase induction motor", *IEEE Uttar Pradesh Section International Conference on Electrical, Computer and Electronics Engineering*, Vol. 46, No. 8, pp. 45-58, 2016.

[11] V. P. Mini, S. Ushakumari, "Rotor fault detection and diagnosis of induction motor using fuzzy logic, "*American Society of Mechanical Journal*, Vol. 87, No. 2, pp. 19-40, 2014.

[12] R. A. Ofosu, A. B. Asiedu-Asante, R. B. Adjei, "Fuzzy logic-based condition monitoring of a 3-phase induction motor", *Proceedings of IEEE AFRICON 2019*, Accra, Ghana, 2020.

[13] A. Gandhi, T. Corrigan, and L. Parsa, "Recent advances in modelling and online detection of stator inter-turn faults in motors", *IEEE Transactions on Industry*, Vol. 40, No.4, pp. 1564-1577, 2012.

[14] T. Kohonen, *MATLAB Implementation and Applications of the Self Organising Map, Unigratia Publishers, Finland, 201pp.*, 2014.

[15] R. K. Rajput, *Electrical Technology*, Laxmi Publishers, Daryaganj, 2nd Edition, 514pp.

[16] S. H. Haggag, M. Ali, and M. Hala, "A new fault detection tool for single phasing of a 3-phase induction motor", *Proceedings of the World Congress on Engineering*, Vol. 2, No. 12, pp. 2 – 5, 2013.

NOMENCLATURE

f_r	ripple frequencies
f_s	stator current harmonic
f	supply frequency
s	slip
k	integer
p	number of pole pairs
d_i	Euclidean distance between sample *x*,
$w_i(t)$	weight vector at iteration *t*
$c(t)$	winning neuron at iteration *t*
QE	quantisation error
T	number of input samples
V_p	peak value of the supply voltage per phase
V_{rms}	RMS voltage rating of the induction motor.
$m_i(t+1)$	adjusted weight vector at iteration *t*
$h_i(t)$	neighbourhood kernel around the winner neuron
x_j	the old weight vectors
V_{Ra}	resultant voltage in phase A
V_a	voltage in phase A

AUTHOR(S) BIOGRAPHY

Robert Agyare Ofosu is a Lecturer in the Electrical and Electronic Engineering Department at the University of Mines and Technology (UMaT), Tarkwa, Ghana. He holds the degrees of BSc Electrical and Electronic Engineering from UMaT and MSc Electrical and Electronic Engineering (Control Engineering Option) from Jomo Kenyatta University of Agriculture and Technology (JKUAT), Kenya and currently pursuing his PhD in Jiangsu University, China. He is a member of the Institute of Electrical and Electronic Engineers (IEEE). His research interests include control engineering, industrial automation, embedded systems, electrical machines and drives and artificial intelligence

 https://doi.org/10.25077/jnte.v12n1.1047.2023

Benjamin Odoi is a Lecturer at the Department of Mathematical Sciences at the University of Mines and Technology (UMaT), Tarkwa, Ghana. He holds the degrees of BSc Mathematics (First Class Hons.), MSc (Applied Statistics), University of Peradeniya (UOP), Sri-Lanka, MPhil Statistics, UMaT, Ghana and PhD in Statistics, UMaT, Tarkwa, Ghana. He also holds a Certificate of Advanced Study in Data Science and Big Data Analytics from Ghana Institute of Management and Public Administration (GI MPA), Ghana. He is a member of African Institute of Mathematical Sciences (AIMS), Statistical Society of Nigeria (PSSN), Professional Applied Statistics Association of Sri Lanka (ASASL). His research areas cover Applied Statistics (Linear Models, Multivariate Statistics, Categorical Data Analysis, Model Selection), Bio statistics, Financial Statistics, Volatility Data Mining and Big Data Analytics.

Daniel Fosu Boateng is a graduate of the University of Mines and Technology, Tarkwa, Ghana. He holds a Bachelor of Science degree in Electrical and Electronic Engineering. His research interests include Control Systems, Power Systems, Telecommunications and Engineering management.

Asaph M. Muhia is a Lecturer in the Department of Electrical and Electronic Engineering at the Jomo Kenyatta University of Agriculture and Technology (JKUAT), Kenya. He holds BSc and MSc degrees in Electrical and Electronic Engineering from JKUAT, Kenya. His area of interests includes control engineering, embedded systems and artificial intelligence.